HHS Public Access

Author manuscript

Nat Biomed Eng. Author manuscript; available in PMC 2017 December 13.

Published in final edited form as:

Nat Biomed Eng. 2017 ; 1: . doi:10.1038/s41551-017-0081.

Host non-inflammatory neutrophils mediate the engraftment of bioengineered vascular networks

Ruei-Zeng Lin[1,2], **Chin Nien Lee**[1,2], **Rafael Moreno-Luna**[1,2], **Joseph Neumeyer**[1], **Breanna Piekarski**[1], **Pingzhu Zhou**[4], **Marsha A. Moses**[2,3,5], **Monisha Sachdev**[3], **William T. Pu**[4,6], **Sitaram Emani**[1,2], and **Juan M. Melero-Martin**[1,2,6,*]

[1]Department of Cardiac Surgery, Boston Children's Hospital, Boston, MA 02115, USA

[2]Department of Surgery, Harvard Medical School, Boston, MA 02115, USA

[3]Vascular Biology Program, Boston Children's Hospital, Boston, MA 02115, USA

[4]Department of Cardiology, Boston Children's Hospital, Boston, MA 02115, USA

[5]Department of Surgery, Boston Children's Hospital, Boston, MA 02115, USA

[6]Harvard Stem Cell Institute, Cambridge, MA 02138, USA

Abstract

Notwithstanding remarkable progress in vascular network engineering, implanted bioengineered microvessels largely fail to form anastomoses with the host vasculature. Here, we demonstrate that implants containing assembled human vascular networks (A-Grafts) fail to engraft due to their inability to engage non-inflammatory host neutrophils upon implantation into mice. In contrast, unassembled vascular cells (U-Grafts) readily engage alternatively polarized neutrophils, which in turn serve as indispensable mediators of vascular assembly and anastomosis. The depletion of host neutrophils abrogated vascularization in U-Grafts, whereas an adoptive transfer of neutrophils fully restored vascularization in myeloid-depleted mice. Neutrophil engagement was regulated by secreted factors and was progressively silenced as the vasculature matured. Exogenous addition of factors from U-Grafts reengaged neutrophils and enhanced revascularization in A-Grafts, a process that was recapitulated by blocking Notch signaling. Our data suggest that the pro-vascularization potential of neutrophils can be harnessed to improve the engraftment of bioengineered tissues.

Tissue engineering holds great promise in regenerative medicine as a solution to the increasing demand for donor organs and tissues [1]. In this context, bioengineering functional

*Corresponding author: Juan M. Melero-Martin, Ph.D., Department of Cardiac Surgery, Boston Children's Hospital, Harvard Medical School, 300 Longwood Ave., Enders 349, Boston, MA 02115, Tel.: (617) 919-3072, Fax: (617) 730-0235, juan.meleromartin@childrens.harvard.edu.

AUTHOR CONTRIBUTIONS

R.-Z.L. and J.M.M.-M. conceived and designed the project. R.-Z.L., C.N.L., R.M.-L., J.N., P.Z., M.S., M.A.M., and J.M.M.-M. performed the experimental work. All authors discussed and analyzed the data and edited the results. W.T.P., B.P., and S.E. provided crucial material. R.-Z.L. and J.M.M.-M. wrote the manuscript.

COMPETING FINANCIAL INTERESTS

The authors declare no competing financial interests.

vascular networks is central [2,3]. The last decade has seen remarkable progress in our collective effort to bioengineer such networks by self-assembly of vascular cells within suitable biomaterials [4–9]. However, efforts remain mostly empirical due in large part to the inability of bioengineered microvessels to connect to the host circulatory system upon implantation. This challenge is similar to that of primary tissues during surgical grafting [10–14]. Indeed, clinical experience with primary tissues has repeatedly shown that inadequate revascularization remains a common outcome, leading to various degrees of graft resorption and failure [15,16]. Therefore, the search for new approaches to advance graft revascularization continues to be a pressing priority in regenerative medicine.

Previous studies have shown that adult neovascularization and angiogenesis rely on myeloid cells [17,18]. Efforts have been primarily focused on the effects of monocytes and macrophages on tumor angiogenesis [19–21]. Nevertheless, studies have also established a prominent role for neutrophils in tumor angiogenesis [22–24]. In grafting models, studies have collectively demonstrated that transplanted hypoxic tissues recruit proangiogenic matrix metalloproteinase (MMP)-9-delivering neutrophils in a vascular endothelial growth factor (VEGF)-dependent manner and that inhibiting neutrophil recruitment impairs in growth of host vessels into the grafts [25,26]. In bioengineered grafts, however, the contribution of neutrophils is largely unknown.

In this study, we sought to determine the extent to which host myeloid cells, in general, and neutrophils, in particular, govern the engraftment of bioengineered vascular networks. To this end, we examined microvasculatures at two contrasting states of maturation. On one hand, we bioengineered graft containing fully-assembled vascular networks embedded in 3-dimensional hydrogel constructs (referred to as *assembled* grafts or A-grafts). These vascular networks mimicked the indolent state of mature microvessels and thus largely failed to spontaneously connect with the host circulation upon implantation. On the other hand, we bioengineered grafts that simply contained an unassembled suspension of vascular cells embedded in a hydrogel (referred to as *unassembled* grafts or U-Grafts), configuration that we have previously shown to effectively produce perfused networks of microvessels following implantation [27,28]. By comparing these two distinct graft models, we found that the inefficient engraftment of A-grafts was due to the inherent inability of their mature microvasculature to engage non-inflammatory host neutrophils, which in U-Grafts served as indispensable mediators of vascularization.

RESULTS

Inefficient engraftment of bioengineered human microvessels

To evaluate engraftment of bioengineered microvessels, we generated grafts containing fully-assembled vascular networks embedded in 3-dimensional constructs (A-grafts). In addition, we prepared grafts that simply contained an unassembled suspension of the same vascular cells (U-Grafts) (Fig. 1a). In both cases, grafts were prepared *in vitro* by combining human endothelial colony-forming cells (ECFCs) with mesenchymal stem cells (MSCs) ($4x10^5$ cells; 1:1 ratio) in gelatin-based hydrogels (GelMA) that were previously shown to be compatible with vascular morphogenesis [5,28]. U-Grafts were suspensions of the cells in the hydrogel at day 0, whereas A-grafts were formed by letting the ECFCs to self-assemble

into mature networks over 7 days *in vitro* (Fig. 1a). We studied the engraftment of both types of grafts following subcutaneous implantation into nude mice. After 7 days *in vivo*, U-Grafts contained an extensive network of perfused microvessels (Fig. 1b). Their lumens expressed h-CD31, confirming the human nature of the endothelium (Fig. 1c), and carried murine erythrocytes, indicating connection with the host circulatory system (Fig. 1b,c; Supplementary Fig. 1). In contrast, the number of perfused human vessels in A-Grafts was insignificant (Fig. 1d). Instead, the ECFCs remained organized as cellular cords but were rarely perfused (Fig. 1b,c). This lack of anastomosis formation by pre-assembled vessels in A-Grafts recapitulated the indolent state observed in the microvasculature of transplanted primary tissues (both murine and human) (Supplementary Fig. 2,3). Thus, this A-Graft/U-Graft model was deemed suitable to study the mechanisms regulating engraftment of a bioengineered vascular network in the absence of tissue parenchyma.

Host neutrophils are indispensable for vascularization

Previously, we recognized that host myeloid cells participate in the vascularization of U-Grafts [29]. In addition, we showed that the hydrogel material used in our grafts is not immunoisolating and that host myeloid cells, including neutrophils, can freely invade our constructs [28]. However, the mechanisms of action and the specific nature of these myeloid subpopulations had yet to be elucidated. Moreover, the role of myeloid cells in the engraftment of A-Grafts was completely unknown. Here, we identified a dynamic presence of three distinct host myeloid subpopulations in U-Grafts: 1) lymphocyte antigen 6 complex, locus G (Ly6G)-/F4/80^{hi} macrophages; 2) Ly6G-/F4/80^{dim} monocytes; and 3) Ly6G+ neutrophils (Supplementary Fig. 4; Fig. 1e). Neutrophil levels peaked prior to the onset of perfusion (~6x10^6 cells/graft at day 2) and then progressively faded as U-Grafts got vascularized, whereas macrophages peaked around day 3 (~3x10^6 cells/graft) and then remained moderately constant (Fig. 1e). Of note, there was a spatially uniform lack of both Ly6G+ neutrophils and macrophages throughout A-Grafts, which was in clear contrast to the abundant presence found in U-Grafts (Fig. 1f–h).

To examine the role myeloid cells in U-Grafts, we devised two separate strategies to deplete either circulating monocytes (α-F4/80 treatment) or neutrophils (α-Ly6G) in recipient mice (Fig. 2a,b; Supplementary Fig. 4). Depletion of circulating monocytes had no significant effect on vascularization; U-Grafts implanted into α-F4/80-treated mice displayed a microvascular density similar to the control group (140.7 ± 30.3 vessels/mm^2 vs. 195.6 ± 19.7 vessels/mm^2 in IgG-treated mice) (Fig. 2c,d). In contrast, depletion of neutrophils was detrimental to vascularization; U-Grafts implanted into α-Ly6G-treated mice had a reduced presence of perfused vessels at day 7 (Fig. 2c) and microvascular density was significantly lower (50.2 ± 6.7 vessels/mm^2) than in the control group (Fig. 2d).

To confirm the pivotal role of neutrophils, we devised an adoptive transfer approach with irradiated mice (radiation effectively depleted >90% circulating myeloid cells for over a week, but it was not lethal; Supplementary Fig. 5). Briefly, U-Grafts were implanted into irradiated mice with or without a transfer of neutrophils from non-irradiated donor mice (Fig. 2e). Transferred neutrophils were an enriched population of mCD11b+/mLy6G+ cells (~95%; Supplementary Fig. 6) obtained with a neutrophil selection kit. U-Grafts implanted

into irradiated mice completely failed to vascularize; however, an adoptive transfer of bone marrow (BM)-derived mLy6G+ cells fully rescued vascularization, enabling formation of extensive networks of perfused blood vessels (Fig. 2f–i). Transfer of blood-derived mLy6G+ cells also rescued vascularization, although to a lesser extent (Fig. 2i). Of note, transfer of BM-derived F4/80+ cells (i.e., monocytes/macrophages) failed to rescue vascularization (Fig. 2f,i; Supplementary Fig. 7), which underscored the distinctive capability of neutrophils. Collectively, these results confirmed that host mLy6G+ neutrophils are indispensable for vascularization in implanted U-Grafts.

Vascularization of U-Grafts in immune-competent mice

To validate the dependency of graft vascularization on host neutrophils in immune-competent hosts, we generated unassembled U-Grafts using murine autologous endothelial cells (ECs) and MSCs isolated from C57BL/6 mice (cells referred to as mECs and mMSCs) (Fig. 3a). These murine cells were isolated from excised subcutaneous tissues that were enzymatically digested and cells were purified by using magnetic beads with antibodies against murine CD31 (for mECs) and platelet-derived growth factor receptor-beta (PDGFRβ) (for mMSCs) via magnetic-activated cell sorting (MACS). Purified mECs and mMSCs were expanded in culture and their phenotype and purity were confirmed, as we previously described [30]. Murine mECs were transduced to express green fluorescent protein (GFP) (referred to as GFP-mECs) and combined with mMSCs to generate U-Grafts, which were then subcutaneously implanted into immunocompetent C57BL/6 mice. Implants were harvested at day 7 and histological (hematoxylin and eosin, H&E) examination revealed that extensive networks of blood microvessels had formed and contained murine erythrocytes, confirming perfusion (Fig. 3b,c). Microvessels were lined by the implanted GFP-mECs as confirmed by GFP immunostaining (Fig. 3e). In addition, GFP+ microvessels were largely covered by alpha-smooth muscle actin (α-SMA)-expressing perivascular cells, indicating stability (Fig. 3e). Taken together, these data demonstrated that U-Grafts containing murine cells (mECs+mMSCs) can form microvascular networks in fully immune-competent hosts (C57BL/6 mice).

Next, we examined whether neutrophils were also indispensable for vascularization in immune-competent hosts (Fig. 3b). As in the previous xenograft model, depletion of neutrophils was also detrimental on vascularization in syngeneic grafts; murine U-Grafts implanted into α-Ly6G-treated C57BL/6 mice completely lacked perfused vessels (neither donor nor host) at day 7 (Fig. 3c,e) and microvascular density was negligible and significantly lower (1.4 ± 1.3 vessels/mm^2) than in the control group (95.6 ± 4 vessels/mm^2) (Fig. 3d).

In addition, we examined the presence of lymphocytes in murine U-Grafts implanted into immune-competent C57BL/6 hosts. To this end, grafts were explanted at day 2, enzymatically digested, and the retrieved cells were analyzed by flow cytometry. We examined the presence of mCD45+/mCD19+ B cells and mCD45+/mCD3+ T cells and found that the presence of both B and T cells in the grafts was minimal (<0.2%) and certainly significantly lower than the myeloid contribution (mCD11b+ cells were ~56.7% at day 2 in syngeneic murine U-Grafts implanted into C57BL/6) (Fig. 3f). Indeed, U-Grafts

implanted into α-Ly6G-treated mice failed to vascularize despite normal levels of circulating lymphocytes.

In summary, we demonstrated that 1) syngeneic murine U-Grafts did vascularize in immune-competent host; 2) neutrophil participation was critical for the vascularization of syngeneic U-Grafts; and 3) lymphocyte presence in the grafts was minimal.

Alternatively polarized neutrophils mediate vascularization

Recent evidence suggest that neutrophils can acquire an alternative non-inflammatory phenotype (referred to as "N2") that mediates tissue remodeling [31]. Here, we compared neutrophils retrieved from explanted U-Grafts to inflammatory neutrophils isolated from lipopolysaccharide (LPS)-containing plugs (Fig. 4a). Neutrophils in U-Grafts did not resemble LPS-activated neutrophils in several respects, including (1) lower mRNA expression of canonical pro-inflammatory genes (namely, *Ccl2*, *Ccl5*, *F4/80*, *Tnf*, *Itgam*, *Csf1*, *Icam1*, *Fas*, and *Il1rn*); (2) higher expression of anti-inflammatory (*Arg1*, *Il4*) and pro-remodeling (*Vegfa*, *Pmepa1*, *Tgfbi*) genes (Fig. 4b); and (3) lower phagocytic activity (Fig. 4c). Previous studies have shown that N2 polarization is mediated via transforming growth factor-beta (TGFβ) signaling [31]. To elucidate the potential role of TGFβ, we adoptively transferred neutrophils lacking TGFβ receptor 2 (*tgfbr2−/−*; from *LysM-Cre::tgfbr2/loxP* donors) into myeloid-depleted (irradiated) nude mice and examined the ability of U-Grafts to vascularize (Fig. 4d–g). *Tgfbr2−/−* neutrophils were not capable of restoring vascularization to the same extent as control neutrophils (34.7 ± 15.9 vessels/mm^2 vs. 100.2 ± 11 vessels/mm^2 with control *LysM-Cre* neutrophils) (Fig. 4g), indicating that the pro-vascularization potential of neutrophils was dependent on *tgfbr2* expression. To further confirm the need for TGFβ signaling, we evaluated the vascularization potential of U-Grafts in mice daily treated with SB432542, a potent and selective inhibitor of the TGF-β type I receptor. We found that treatment with SB432542 impaired the formation of perfused vascular networks. Indeed, the number of perfused vessels at day 7 in U-Grafts from SB432542-treated mice was insignificant (Fig. 4j); ECFCs appeared organized as cellular cords, but these cords were rarely perfused (Fig. 4h,i).

Taken together, our results show that U-Graft's neutrophils distinctively displayed a non-inflammatory phenotype that was consistent with the N2 phenotype; this alternative polarization was dependent on TGFβR/TGFβ signaling, and in turn was essential for neutrophil pro-vascularization function. Moreover, blocking TGFβ signaling via exogenous provision of SB432542 completely abrogated U-Graft vascularization.

Neutrophils activity is regulated by secreted factors

To gain further insight into how grafts engage host neutrophils, we collected daily samples of conditioned media (CM) from U-Grafts over 8 days *in vitro* (i.e., until they became A-Grafts) (Fig. 5a). Subcutaneous plugs containing CM from U-Grafts robustly recruited neutrophils in nude mice (Fig. 5b) - note that neutrophil recruitment by CM(U-Grafts) was significantly higher than by CM(ECFCs) and CM(MSCs) separately (Supplementary Fig. 8). However, plugs containing CM from A-Grafts had no detectable neutrophils, a decline that occurred progressively and coincided with the assembly of cells into vascular networks (Fig.

5c). Moreover, human cells retrieved from A-Grafts could immediately regain ability to recruit neutrophils when used in new U-Grafts (Supplementary Fig. 8). Thus, neutrophil recruitment was mediated by secreted factors and was directly related to the state of the vascular cells (assembled vs. unassembled) within the grafts.

Next, we studied whether exposing A-Grafts to CM from U-Grafts could thus enhance engraftment of assembled bioengineered vessels (Fig. 5d). First, we observed that A-Grafts that were simply impregnated once with CM(U-Graft) at the time of implantation contained significantly more neutrophils at day 2 than the control (Fig. 5e). In addition, A-Grafts + CM(U-Graft) contained an extensive network of perfused microvessels at day 7 (Fig. 5f,g). Moreover, the extent to which CM(U-Grafts) induced revascularization of A-Grafts was significantly higher than that of CM(ECFCs) and CM(MSCs) separately (Supplementary Fig. 9). Examination of human-specific (h-CD31+) lumens revealed that A-Grafts + CM(U-Graft) comprised perfused human microvessels that carried murine erythrocytes, indicating successful connection of pre-assembled vessels with the host circulatory system (Fig. 5h). In contrast, A-Grafts + basal-M had a significantly lower number of perfused human lumens at day 7 (8.7 ± 0.6 vessels/mm^2 vs. 31.2 ± 7.0 vessels/mm^2 in A-Grafts + CM(U-Graft)) (Fig. 5i). Instead, human ECFCs remained organized as non-perfused cellular cords (Fig. 5f,h). Thus, a critical difference between U-Grafts and A-Grafts resides in the presence or absence of secreted factors that recruit and activate host neutrophils, which in turn modulate graft vascularization. Importantly, exogenous provision of factors from U-Grafts could reengage neutrophils and enhance revascularization in A-Grafts.

Inhibition of Notch signaling promotes revascularization

Microvascular stability is associated with activation of Notch in the endothelium [32,33]. However, the relation between endothelial Notch signaling and neutrophil activity in the context of grafting remains largely unexplored. mRNA expression of *NOTCH1*, as well as several downstream mediators of Notch signaling (*HEY1*, *HEY2*, *HES1*, and *HES5*), was upregulated in ECFCs from A-Grafts compared to U-Grafts (Fig. 6a). Moreover, expression of human-specific genes (*NOTCH1, HEY1*, *HEY2*, and *HES1*) were all significantly up-regulated by the human cells in implanted U-Grafts over a 7-day period, confirming the association between vascular maturity and Notch expression *in vivo* (Fig. 6a). Inversely, expression levels of several cytokines with neutrophil chemoattractant activity (namely, *CXCL1*, *CXCL8*, and *IL6*) were downregulated in ECFCs from A-Grafts (Fig. 6b), which coincided with reduced neutrophil presence. Cytokine analyses of CM confirmed widespread downregulation of numerous neutrophil chemoattractants in A-Grafts vs. U-Grafts (Fig. 6c). Of note, exposing A-Grafts to the Notch inhibitor DAPT (a γ-secretase inhibitor) for 24 h reactivated the expression of several cytokines (most significantly CXCL1, CXCL8, and IL6) (Fig. 6c), suggesting a relationship between Notch activation and the secretion of neutrophil chemoattractants by the vasculature. Moreover, the use of antibodies to specifically block each of the identified cytokines (most significantly IL6 and CXCL8) in CM from U-Grafts interfered with the recruitment of neutrophils into subcutaneous plugs (Fig. 6d), whereas plugs containing CM from DAPT-treated A-Grafts recruited significantly more neutrophils than plugs with CM from untreated A-Grafts (Fig. 6d).

To further elucidate the significance of secreted cytokines, we examined the effect of a non-peptide CXCR2 antagonist (SB225002) on the vascularization of U-Grafts. CXCR2 is a receptor for both CXCL8 and CXCL1, and previous studies have shown that SB225002 effectively inhibits neutrophil chemotaxis in response to CXCL8 both *in vitro* and *in vivo* [34]. Indeed, SB225002 treatment significantly impaired neutrophil presence in our implanted U-Grafts at day 2 (Fig.6e). Importantly, U-Grafts that were implanted into SB225002-treated mice had significantly lower microvessel densities than those implanted into control animals (Fig.6f). To put this result in context, SB225002-treatment produced a reduction in vascularity that was similar to the reduction produced by depletion of host neutrophils with α-Ly6G antibody (Fig. 6f). Moreover, a combination treatment with α-Ly6G + SB225002 further reduced microvessel density in U-Grafts (down to ~8 vessels/mm^2), although the differences in reduction between the combination and each individual treatment were not statistically significant. Nevertheless, this additional reduction in microvessel density due to the combination treatment might suggest participation of an additional type of host CXCR2+ cells that, together with neutrophils, mediate graft vascularization.

Next, we examined whether deactivation of Notch could rescue the inherent lack of revascularization in A-Grafts. To this end, we incubated A-Grafts with DAPT for 24 h ahead of their implantation into mice. Compared to untreated grafts, DAPT-treated A-Grafts had significantly more neutrophils at day 2 (Fig. 6g). In addition, DAPT-treated A-Grafts contained more extensive networks of perfused microvessels that were unequivocally human after 7 days *in vivo* (Fig. 6h–j), and the difference in microvascular density between DAPT-treated and untreated grafts was significant (Fig. 6k). Importantly, human vessels in DAPT-treated A-Grafts were surrounded by perivascular α-SMA+ cells (Supplementary Fig. 10), indicating that the transient inhibition of Notch signaling did not compromise proper perivascular coverage.

DISCUSSION

In this study, we sought to determine the cellular mechanisms impairing engraftment of bioengineered human vascular networks. We showed that the inefficient formation of anastomoses in assembled microvessels (A-Grafts) is due to an inherent inability of mature vessels to engage a subset of alternatively polarized (non-inflammatory) host neutrophils at the implantation site. This contrasted with grafts comprising a non-assembled suspension of vascular cells (U-Grafts), which rapidly engage neutrophils to mediate proper vascularization. Depletion of host neutrophils significantly abrogated vasculogenesis in U-Grafts, whereas an adoptive transfer of neutrophils restored vascularization in myeloid-depleted mice. The dependency on host neutrophils was complete and corroborated in both syngeneic (murine grafts implanted into mouse) and xenograft (human in mouse) models. Neutrophil recruitment and activation were controlled by factors secreted from the implanted vascular cells, a process initially upregulated in unassembled U-Grafts but progressively silenced as the vasculature matured. This mechanism of progressive neutrophil disengagement could explain the inactive nature of assembled microvasculatures - both bioengineered and primary - with regards to their capacity to engraft and connect with host vessels.

Emerging evidence indicate that neutrophils can comprise two distinct subpopulations with different polarized phenotypes: 1) a canonical pro-inflammatory phenotype (referred to as "N1"); and 2) an alternative anti-inflammatory, pro-remodeling, phenotype ("N2") [31,35,36], resembling the well-established "M1–M2" macrophage paradigm. N2 polarization has been substantiated in a variety of tumor models, and it involves TGFβ-mediated activation (TGFβ inhibition produces a shift to N1, and in turn acquisition of antitumor activity), followed by downregulation of pro-inflammatory genes and expression of both anti-inflammatory factors and proangiogenic mediators [31,37,38]. Recently, the contribution of alternatively polarized N2 neutrophils has also been described in non-neoplastic events, including brain stroke [39] and myocardial infarction [40]. However, their participation in tissue grafting was not previously described. Here, we identified that graft neutrophils displayed a phenotype that was consistent with the notion of an alternative N2 polarization in several respects including low expression of canonical pro-inflammatory genes, high expression of anti-inflammatory and pro-remodeling genes, low phagocytic activity, and TGFβR2-mediated activation. We also found that adoptive transfer of neutrophils from bone marrow restored vascularization in myeloid-depleted mice to a better extent than blood neutrophils, which is consistent with published evidence of immature non-inflammatory neutrophils (equivalent to "N2" neutrophils) being more abundant in the bone marrow than in circulation [37].

Though our study focused on the role of neutrophils in graft vascularization, our implants also contained host macrophages and monocytes. Macrophage presence was expected in light of their role as cellular chaperones for vascular anastomosis during angiogenesis [41]. Furthermore, macrophage-neutrophil interdependency during angiogenesis is well established [42–44]. In our studies, the indispensable role of neutrophils in graft vascularization did not preclude participation of host macrophages, which were also abundant at the onset of perfusion. However, we demonstrated that in the absence of neutrophils, macrophage involvement in vascularization was undoubtedly insufficient. With regard to host monocytes, our results were equally conclusive: depletion of circulating monocytes had no appreciable effect on graft vascularization and adoptive transfer of BM-derived F4/80+ cells could not restore normal vascular activity in myeloid-depleted mice. Lastly, our results with α-Ly6G (neutrophil depletion) + SB225002 (CXCR2 inhibitor) revealed that this combination reduced vascularization in U-Grafts more than either of the treatments separately, although the differences were not statistically significant. Nevertheless, the additional reduction in microvessel density with the combination treatment might indicate participation of an additional type of host CXCR2+ cells in vascularization, suggesting that neutrophils are likely not solely responsible for the vascularization of the grafts. Further research is warranted to confirm a role and to elucidate the nature of additional host CXCR2+ cells that may contribute to the process of graft vascularization.

Prior to our study, the mechanisms regulating engraftment of bioengineered microvessels remained essentially unexplored. Nevertheless, some recent studies did report positive integration between engineered and host vessels. Baranski and colleagues bioengineered vascular networks by the assembly of human ECs (HUVECs) and murine embryonic perivascular cells (10T1/2 cell line), and demonstrated perfusion with host blood upon implantation into the intraperitoneum of nude mice [45]. More recently, Riemenschneider et. al. constructed patches containing self-assembled microvessels formed by co-entrapment of

ECFCs and human fetal brain pericytes in fibrin gel. These patches were sutured onto the epicardial surface of the hearts of athymic rats following permanent ligation of the left anterior descending artery; ~25% of the bioengineered vessels were found perfused [46]. Thus, the poor engraftment seen with our bioengineered vessels might seem inconsistent with these previous reports. However, it is important to note that the sources of perivascular cells in the aforementioned studies were embryonic and fetal tissues, respectively. Considering that xenograft studies have shown that embryonic (but not adult) vasculature can form spontaneous connections with the host [47], it is conceivable that the sole presence of fetal cells could facilitate the formation of anastomoses. In any case, bioengineering tissues with non-autologous fetal cells poses additional challenges related to immune tolerance and thus may have reduced translational potential. Further studies are warranted to elucidate if host neutrophils also mediate vascular anastomoses in bioengineered vessels that use embryonic/fetal cells.

Harnessing the pro-vascularization potential of neutrophils could become the basis for a new strategy to engraft bioengineered tissues. Moreover, this approach could potentially benefit grafting clinical procedures that critically rely on adequate revascularization. Clinical and preclinical studies have repeatedly shown that perfused vessels in adult primary tissue grafts are almost exclusively originated by infiltration of host vessels. However, this process of revascularization poses two main constraints on the grafts: (1) inadequate blood supply to the center, which leads to necrosis and resorption; and (2) irreversible loss of graft endogenous vasculature. The latter is important because mounting evidence indicates that most tissues have highly specialized endothelium that regulates homeostatic and regenerative processes in a tissue-specific manner [48–52]. Thus, loss of endogenous vessels could contribute to long-term malfunctioning of the grafts. Enabling a robust integration of the graft microvasculature could eliminate the abovementioned constraints. In light of our study, new strategies to improve microvascular engraftment could focus on harnessing non-inflammatory neutrophils by exposing the grafts to specific exogenous vascular factors and/or blocking Notch signaling, which could reactivate endogenous mechanisms in mature vessels. We anticipate that forthcoming studies will address whether engaging host neutrophils would indeed improve revascularization of primary tissue grafts and how this strategy would ultimately affect parenchymal function in the engrafted tissues.

METHODS

Mice

Nu/nu (BALB/c background; Massachusetts General Hospital) and C57BL/6 males (Jackson Laboratory) were used for implantation of human and syngeneic murine grafts, respectively, unless stated otherwise. Rosa26^{fsTrap} (129S1 background) and Cdh5(Pac)-CreERT2+ (C57BL/6 background) transgenic mice [53,54] were interbred and offspring were given two consecutive intragastric injections of 50 μl tamoxifen (2 mg/ml in sunflower seed oil) on postnatal day P1 and P2 to induce Cre recombinase activity. The resulting Rosa26^{fsTrap};Cdh5(Pac)-CreERT2+ mice served as donors and their tissues expressed eGFP-L10a fusion protein in endothelial cells. For myeloid-specific *tgfbr2* deletions, LysM-Cre transgenic mice (Jackson Laboratory, JAX004781) were interbred with conditional

Tgfbr2$^{lox/lox}$ mutants (JAX012603; both C57BL/6 background). The offspring were interbred again and genotyped to select homozygous *tgfbr2*$^{-/-}$ (LysM-Cre$^{+/+}$ Tgfbr2$^{lox/lox}$) alleles. The myeloid-specific deletions of *tgfbr2* were confirmed by PCR. Animal experiments were conducted under a protocol approved by the Institutional Animal Care and Use Committee at Children's Hospital Boston in an AAALAC-approved facility.

Transplantation of primary murine tissue grafts

6-weeks-old Rosa26^{fsTrap};Cdh5(Pac)-CreERT2+ transgenic mice served as donors and were perfused with PBS before being euthanized. Myocardium, liver and kidney were harvested and trimmed into 3x3x3 mm^3 grafts. Tissue grafts were then surgically implanted into subcutaneous space on the back of nude mice with 50-μL of collagen-fibrin gel (3 mg/mL of bovine collagen, 30 μg/mL of human fibronectin, 25mM HEPES, 10% 10x DMEM, 10% FBS, and 3 mg/mL of fibrinogen, pH neutral; mixed with 10 μL of 10 U/mL thrombin immediately before implantation). After 7 days *in vivo*, fluorescein isothiocyanate (FITC)-conjugated *Griffonia Simplicifolia Lectin I (GSL I) isolectin B4* in saline (Iso-B4; 50 μg/100 μL/mouse) was infused intravenously 10 min before euthanasia. Grafts were explanted and subjected to histological analyses. Anti-FITC and anti-GFP antibodies were used to stain perfused and donor vessels, respectively.

Transplantation of primary human myocardial tissue grafts

Discarded normal human right ventricular myocardial tissues were obtained during clinically-indicated procedures in accordance with an Institutional Review Board-approved protocol. Myocardial tissues were immediately transported to the laboratory in cold sterile saline, trimmed into 3x3x3 mm^3 cubes, and surgically implanted (subcutaneously) into nude mice. 50-μL of collagen-fibrin gel was added around myocardial grafts to improve integration with host tissues. 7 days after implantation, FITC-conjugated *Ulex Europaeus Agglutinin-I* in saline (UEA-I; 50 μg/100 μL/mouse) was infused intravenously 10 min before euthanasia. Grafts were explanted and subjected to histological analyses. Perfused human vessels were stained by biotinylated-anti UEA-I antibody and streptavidin-TexasRed.

Isolation and culture of human MSCs and ECFCs

Human MSCs were isolated from the mononuclear cell fraction of bone marrow aspirates as previously described [7]. MSCs were cultured on uncoated plates using MSC-medium: MSCGM (Lonza) supplemented with 10% MSC-qualified FBS (Hyclone), 1x glutamine-penicillin-streptomycin (GPS; Invitrogen). All experiments were carried out with MSCs between passages 6–10. Human ECFCs were isolated from umbilical cord blood samples in accordance with an Institutional Review Board-approved protocol as previously described [27]. ECFCs were cultured on 1% gelatin-coated plates using ECFC-medium: EGM-2 (except for hydrocortisone; Lonza) supplemented with 20% FBS, 1x GPS. All experiments were carried out with ECFCs between passages 6–8. DsRed-labeled ECFCs were generated by lentiviral infection with a pLVX-DsRed vector (Clontech) and selected with puromycin (2 μg/mL) [5].

Fabrication and implantation of bioengineered grafts

Photopolymerizable methacrylated gelatin (GelMA) hydrogel was synthesized as previously described [5]. GelMA prepolymer solution was prepared in PBS at 80°C (5 w/v% final) with photoinitiator Irgacure 2959 (0.5 w/v%; CIBA Chemicals), and then allowed to cool down to 37°C in a water bath. ECFCs and MSCs ($4x10^5$ total; 1:1 ratio) were suspended in 200 μL of GelMA solution and the mixture was polymerized by exposure to 7.5 mW/cm^2 UV light for 15 s at 37°C. Polymerized cell-laden constructs were referred to as unassembled grafts or U-Grafts. Alternatively, on indicated experiments, U-Grafts were constructed with ice-cold Phenol Red-free Matrigel (BD Bioscience). Assembled grafts or A-Grafts were constructed by culturing U-Grafts *in vitro* for 7 days using EGM-2 with 5% FBS. A-Grafts contained easily observable, fully-assembled vascular networks. Both, U-Grafts and A-Grafts were subcutaneously implanted into back of 6-week-old male athymic nu/nu mice for engraftment studies. On specified experiments, DsRed-labeled ECFCs were used to visualize the formation of assembled vascular networks in A-Grafts. For Notch signaling inhibition studies, A-Grafts were treated with the γ-secretase inhibitor DATP (10 μM in EGM-2 with 5% FBS) for 24 h prior to implantation; A-Grafts cultured for 8 days in EGM-2 with 5% FBS served as a control. To evaluate host myeloid cell recruitment, grafts were explanted two days after implantation and subjected to flow cytometric and histological analyses. To assess vascularization, grafts were explanted 7 days after implantation and were subjected to histological analysis. On indicated experiments, FITC-conjugated UEA-I (50 μg/100 μL per mouse) was injected intravenously 10 min before euthanasia to label perfused human vessels.

Isolation and culture of murine MSCs and ECs

Subcutaneous white fat pads were excised from euthanized C57BL/6 mice, minced, and digested (1 mg/mL collagenase A, 2.5 U/mL dispase, 126 μM calcium chloride, and 80 μM magnesium sulfate in DMEM containing 1% FBS) for 1 hr at 37°C. The stromal vascular fractions (SVFs) were obtained after removal of mature adipocytes by centrifugation (450 g for 10 min) and the lysis of erythrocytes with ammonium chloride solution. The SVFs were incubated with a FITC-conjugated anti-mouse CD45 antibody, followed by anti-FITC magnetic microbeads (Miltenyi Biotec), and passed through magnetic columns (Miltenyi Biotec). The mCD45- cell fraction was then incubated with a PE-conjugated anti-mPDGFR-β or anti-mCD31 antibodies, followed by anti-PE magnetic microbeads, and passed through magnetic columns. The purified mCD45-/mPDGFR-β+ murine MSCs (mMSCs) were cultured on uncoated tissue culture dishes using MSC-medium. The purified mCD45-/mCD31+ ECs (mECs) were cultured on fibronectin-coated tissue culture dishes using ECFC-medium. mECs were then transduced with lentivirus (pLenti-CMV-GFP; Addgene) to express GFP under CMV promoter (referred to as GFP-mECs). All experiments were carried out with mMSCs at passage 3 and GFP-mECs at passage 12.

Syngeneic murine model of graft vascularization

C57BL/6-derived mMSCs and GFP-mECs were implanted in collagen-fibrin gel ($2x10^6$ total; 3:2 ratio; 200 μL) subcutaneously into host C57BL/6 males as U-Grafts in a syngeneic murine model. To evaluate host myeloid cell recruitment, grafts were explanted two days

after implantation and subjected to flow cytometric analyses. To assess vascularization, grafts were explanted 7 days after implantation and were subjected to histological analysis. Immunofluorescent staining of GFP indicated the grafting of donor GFP-mECs.

Histology and immunohistochemistry

Explanted grafts were fixed overnight in 10% buffered formalin, embedded in paraffin and sectioned (7-μm-thick). Hematoxylin and eosin (H&E)-stained sections were examined for the presence of erythrocyte-filled blood vessels. For immunostaining, sections were deparaffinized and antigen retrieval was carried out with tris-EDTA buffer (10 mM Tris-Base, 2 mM EDTA, 0.05% Tween-20, pH 9.0) or citric buffer (10 mM sodium citrate, 0.05% Tween 20, pH 6.0). Sections were then blocked for 30 min in 5–10% blocking serum and incubated with primary antibodies overnight at 4°C. Horseradish peroxidase-conjugated mouse secondary antibody (1:200; Vector Laboratories) and 3,3′-diaminobenzidine (DAB) were used for detection of h-CD31, followed by hematoxylin counterstaining and Permount mounting. Fluorescent staining was performed using fluorescently-conjugated secondary antibodies (1:200) followed by DAPI counterstaining (Vector Laboratories). When indicated, h-vimentin staining was used to identify human cells (both ECFCs and MSCs) (please note that the anti-h-vimentin antibody used is very specific to human vimentin and does not react with murine cells and tissues) [7]. Primary and secondary antibodies are detailed in Supplementary Table 1.

Microvessels density

Microvessel density was reported as the average number of erythrocyte-filled vessels (vessels/mm^2) in H&E-stained sections from the middle of the implants as previously described [7]. The entire area of each section was analyzed. On specified experiments, human-specific microvessel density was quantified by evaluation of slides immunostained for human-specific CD31 (h-CD31). Perfused microvessel density was measured by injection of FITC-labeled lectins (UEA-1 or Iso-B4) before euthanizing graft-bearing mice, followed by staining of lectin-labeled vessels with anti-UEA-1 or anti-FITC antibodies.

Cell retrieval and flow cytometry

Grafts were removed from euthanized mice and cells were retrieved by enzymatic (1 mg/mL collagenase and 2.5 U/mL dispase) digestion for 1 h at 37 °C. Retrieved cells were then prepared into single-cell suspensions. In indicated experiments, retrieved cells were sorted into h-CD31+ and h-CD31− cells by magnetic-activated cell sorting (MACS) using magnetic beads (DynaBead) coated with anti-human CD31 antibodies. Retrieved cells were also stained for flow cytometry and analyzed using a Guava easyCyte 6HT/2L flow cytometer (Millipore Corporation, Billerica, MA) and FlowJo software (Tree Star Inc., Ashland, OR). Antibody labeling was carried out for 20 min on ice followed by 3 washes with PBS supplemented with 1% BSA and 0.2 mM EDTA. Cell staining was followed by fixation with 1% paraformaldehyde. To identify murine myeloid population, cell suspensions were incubated with PerCP-conjugated anti-mouse CD45, PE-conjugated anti-mouse F4/80 and FITC-conjugated anti-mouse Ly6G with concentrations indicated in Supplementary Table 1. Murine neutrophils were identified as mCD45+/mLy6G+ cells. Murine monocytes and macrophages were identified as mCD45+/mLy6G-/mF4/80^{dim} cells

and mCD45+/mLy6G-/mF4/80^{high} cells, respectively. To identify murine lymphocytes, cell suspensions were incubated with PerCP-conjugated anti-mouse CD45, PE-conjugated anti-mouse CD19 and FITC-conjugated anti-mouse CD3e. Murine T cells and B cells were identified as mCD45+/mCD3+ and mCD45+/mCD19+ cells, respectively. In indicated experiments, retrieved cells were sorted into mCD45+/mLy6G+ (neutrophils) and mCD45+/mLy6G- cells by fluorescence-activated cell sorting (FACS) using a FACSAria II 5-LASER sorter system (BD Bioscience). Sorted cells were analyzed immediately for gene expression by qPCR.

Myeloid cell depletion

Antibodies were administered intraperitoneally according to the schedule described in Fig. 2a. Rat anti-mouse Ly-6G (clone 1A8; Bio X Cell) antibodies were administered at 200 μg/mouse 2 days before U-grafts implantation, and then every other day at 100 μg/mouse. Rat anti-mouse F4/80 (clone CI:A3-1; Bio X Cell) antibodies were administered at 400 μg/mouse 2 days before U-grafts implantation, and then every day at 200 μg/mouse. Daily injection of rat IgG (200 μg/mouse) served as control. Monocyte and neutrophil depletion was confirmed in blood samples by flow cytometry.

Myeloid adoptive transfer model

Circulating myeloid cells were depleted from recipient mice by two 4Gy gamma irradiation sessions at days −4 and 0. mLy6G+ neutrophils or mF4/80+ cells (~10^7 cells) from non-irradiated donor mice were adoptively transferred by injection at the implantation sites in recipient mice and at the same time of U-Graft implantation (day 0). Donor neutrophils were isolated from either bone marrow or blood using a murine neutrophil isolation kit that enriches for CD11b+/Ly6G+ cells (Miltenyi Biotec; negative selection using a cocktail that contains anti CD5, CD45R/B220, CD49b, CD117/c-kit, F4/80 and Ter119 antibodies). Donor mF4/80+ cells were isolated from bone marrow by magnetic-activated cell sorting (MACS) using magnetic beads (Miltenyi Biotec) coated with anti-mF4/80 antibodies.

Generation of conditioned media

Samples of conditioned media (CM) were collected daily from U-Grafts over 8 days *in vitro* (i.e., until they became A-Grafts). To this end, grafts were cultured in 3-mL tubes with 500 μL of EBM-2, 5% FBS media refreshed every 24 h. Collected CM samples were filtered (0.2 μm) and then concentrated 10-fold (Amicon Ultra centrifugal filters; 3 kDa cut off; Millipore). In indicated experiments, A-Grafts were impregnated with CM from U-Grafts. To this end, A-Grafts were placed on clean kimwipes (2x2 cm^2) and then concentrated CM (50 μL) from U-Grafts was added on top of the grafts slowly to allow a replacement of culture medium by capillary force. Impregnated A-Grafts were immediately implanted into recipient mice. A-Grafts impregnated in basal media (basal-M: EBM-2, 5% FBS) and CM from grafts containing only ECFCs or MSC alone served as controls.

Neutrophil recruitment plug assay

Concentrated CM (50 μL) was mixed with 200-μL of Matrigel and injected subcutaneously into nu/nu mice. After 2 days, plugs were explanted and infiltrated cells were retrieved by

enzymatic digestion and subjected to flow cytometric analysis. Concentrated basal media (basal-M: EBM-2, 5% FBS) served as control. In indicated experiments, neutralizing antibodies against IL6, CXCL1 or CXCL8 (5 μg/antibody/plug) were added to concentrated CM 30 min prior to implantation. Individual neutralizing antibodies and the combination of three were compared.

CXCR2 antagonist treatment

CXCR2 antagonist SB225002 (Sigma) was administered at 7.5 mg/kg intraperitoneally 30 mins before U-grafts implantation, and then every day until day 7. Neutrophil recruitment at day 2 and graft vascularization at day 7 were measured as described before. Daily injection of saline served as control. In selected experiments, SB225002 treatment was combined with rat anti-mouse Ly-6G treatment (clone 1A8; administered as described above) to study the combined effect on U-Graft vascularization.

TGF-β receptor inhibitor treatment

U-Grafts were implanted in mice systemically treated with a TGF-β receptor inhibitor (SB432542; 10 mg/kg of animal weight; daily intraperitoneal injection). Mice receiving saline injections served as controls. Grafts were harvested at day 7 to evaluate vascularization.

LPS plug assay

Lipopolysaccharides (LPS; 10 μg; from E. coli 0111:B4; Sigma) were mixed with 200-μL Matrigel and was injected subcutaneously into nu/nu mice. After 1 day, plugs were explanted, infiltrated cells were retrieved, and neutrophils were sorted by FACS for analysis.

Phagocytosis assay

Cells were retrieved from U-Grafts or LPS plugs 24 h after implantation and were then incubated with GFP-expressing *E. coli*. for 30 min. Cells were washed twice in PBS and free bacteria were removed by centrifugation (300 rpm). Cells were analyzed by flow cytometry and immunofluorescence. Murine neutrophils were identified as mCD45+/mLy6G+ cells and phagocyted *E. coli* as GFP+ bacteria.

Human cytokine protein array

The presence of selected cytokines was evaluated in samples of CM with human cytokine protein arrays (R&D Systems Inc.) according to the manufacturer's instructions. Antigen-antibody complexes were visualized using LumiGLO substrate (Kirkegaard & Perry Laboratories, Inc.) and chemiluminescent sensitive film (Kodak). Densitometry was performed by image analysis (ImageJ) to estimate the amount of protein present in each sample.

Quantitative RT-PCR

Quantitative RT-PCR (qRT-PCR) was carried out in RNA lysates prepared from either explanted grafts, cells in culture, or cells retrieved from grafts. Total RNA was isolated with a RNeasy kit (QIAGEN) and cDNA was prepared using reverse transcriptase III

(Invitrogen), according to the manufacturer's instructions. Multigene transcriptional profiling, a form of qRT-PCR, was used to determine the number of mRNA copies per cell normalized to ribosomal 18S rRNA abundance, as previously described [55]. Human-specific gene expression in explanted grafts were measured using human-specific primers and normalized to human beta actin (ACTB) expression. Real-time PCR primer sequences are displayed in Supplementary Table 2. Heat maps were generated using Gene-E software package from the Broad Institute (www.broadinstitute.org/cancer/software/GENE-E/).

Microscopy

Images were taken using an Axio Observer Z1 inverted microscope (Carl Zeiss) and AxioVision Rel. 4.8 software. Fluorescent images were taken with an ApoTome.2 Optical sectioning system (Carl Zeiss) and 20x/0.8 or 40x/1.4 oil objective lens. Non-fluorescent images were taken with an AxioCam MRc5 camera using a 40x/1.4 objective oil lens.

Statistical analyses

Unless otherwise stated, data were expressed as mean ± standard deviation of the mean (s.d.). For comparisons between two groups, means were compared using unpaired two-tailed Student's t-tests. Comparisons between multiple groups were performed by ANOVA followed by Bonferroni's post-test analysis. Samples size, including number of mice per group, was chosen to ensure adequate power and were based on historical data. No exclusion criteria was applied for all analyses. No specific methods of randomization were applied to group/animal allocation. Investigators were not blinded to group allocation. All statistical analyses were performed using GraphPad Prism v.5 software (GraphPad Software Inc.). $P<0.05$ was considered statistically significant.

Data availability

The authors declare that all data supporting the findings of this study are available in the paper and its Supplementary Information.

Supplementary Material

Refer to Web version on PubMed Central for supplementary material.

Acknowledgments

We thank Dr. Shou-Ching S. Jaminet and Dan Li (Center for Vascular Biology, Beth Israel Deaconess Medical Center, Boston) for quantitative reverse transcription-polymerase chain reaction analyses. Histology was supported by Core Facility of the Dana-Farber/Harvard Cancer Center (P30 CA06516). This work was supported by National Institutes of Health grants R00EB009096, R01AR069038, R01HL128452, and R21AI123883 to J. M.-M.

References

1. Griffith LG, Naughton G. Tissue Engineering--Current Challenges and Expanding Opportunities. Science. 2002; 295:1009–1014. [PubMed: 11834815]
2. Rouwkema J, Rivron NC, Van Blitterswijk CA. Vascularization in tissue engineering. Trends Biotechnol. 2008; 26:434–441. [PubMed: 18585808]
3. Novosel EC, Kleinhans C, Kluger PJ. Vascularization is the key challenge in tissue engineering. Adv Drug Deliv Rev. 2011; 63:300–311. [PubMed: 21396416]

4. Schechner JS, et al. In vivo formation of complex microvessels lined by human endothelial cells in an immunodeficient mouse. Proc Natl Acad Sci USA. 2000; 97:9191–9196. [PubMed: 10890921]
5. Chen YC, et al. Functional Human Vascular Network Generated in Photocrosslinkable Gelatin Methacrylate Hydrogels. Adv Funct Mater. 2012; 22:2027–2039. [PubMed: 22907987]
6. Jain RK, Au P, Tam J, Duda DG, Fukumura D. Engineering vascularized tissue. Nat Biotechnol. 2005; 23:821–823. [PubMed: 16003365]
7. Melero-Martin JM, et al. Engineering robust and functional vascular networks in vivo with human adult and cord blood-derived progenitor cells. Circ Res. 2008; 103:194–202. [PubMed: 18556575]
8. Traktuev DO, et al. Robust functional vascular network formation in vivo by cooperation of adipose progenitor and endothelial cells. Circ Res. 2009; 104:1410–1420. [PubMed: 19443841]
9. Chen X, et al. Rapid anastomosis of endothelial progenitor cell-derived vessels with host vasculature is promoted by a high density of cotransplanted fibroblasts. Tissue Eng Part A. 2010; 16:585–594. [PubMed: 19737050]
10. Moisidis E, Heath T, Boorer C, Ho K, Deva AK. A Prospective, Blinded, Randomized, Controlled Clinical Trial of Topical Negative Pressure Use in Skin Grafting. Plast Reconstr Surg. 2004; 114:917–922. [PubMed: 15468399]
11. Larry MW, Eber LLS. Considerations in nerve repair. Proceedings (Baylor University Medical Center). 2003; 16:152–156. [PubMed: 16278731]
12. Giannoudis PV, Dinopoulos H, Tsiridis E. Bone substitutes: An update. Injury. 2005; 36:S20–S27. [PubMed: 16188545]
13. Kølle S, Fischer-Nielsen A, Mathiasen AB, Elberg JJ. Enrichment of autologous fat grafts with ex-vivo expanded adipose tissue-derived stem cells for graft survival: a randomised placebo-controlled trial. Lancet. 2013; 13:1113–1120.
14. Mohr FW, et al. Coronary artery bypass graft surgery versus percutaneous coronary intervention in patients with three-vessel disease and left main coronary disease: 5-year follow-up of the randomised, clinical SYNTAX trial. Lancet. 2013; 381:629–638. [PubMed: 23439102]
15. Serruys PW, et al. Percutaneous Coronary Intervention versus Coronary-Artery Bypass Grafting for Severe Coronary Artery Disease. N Engl J Med. 2009; 360:961–972. [PubMed: 19228612]
16. Rogers GF, Greene AK. Autogenous bone graft: basic science and clinical implications. J Craniofac Surg. 2012; 23:323–327. [PubMed: 22337435]
17. Nahrendorf M, et al. The healing myocardium sequentially mobilizes two monocyte subsets with divergent and complementary functions. J Exp Med. 2007; 204:3037–3047. [PubMed: 18025128]
18. Grunewald M, et al. VEGF-induced adult neovascularization: recruitment, retention, and role of accessory cells. Cell. 2006; 124:175–189. [PubMed: 16413490]
19. Shojaei F, Zhong C, Wu X, Yu L, Ferrara N. Role of myeloid cells in tumor angiogenesis and growth. Trends Cell Biol. 2008; 18:372–378. [PubMed: 18614368]
20. De Palma M, et al. Tie2 identifies a hematopoietic lineage of proangiogenic monocytes required for tumor vessel formation and a mesenchymal population of pericyte progenitors. Cancer Cell. 2005; 8:211–226. [PubMed: 16169466]
21. De Palma M, Venneri MA, Roca C, Naldini L. Targeting exogenous genes to tumor angiogenesis by transplantation of genetically modified hematopoietic stem cells. Nat Med. 2003; 9:789–795. [PubMed: 12740570]
22. Nozawa H, Chiu C, Hanahan D. Infiltrating neutrophils mediate the initial angiogenic switch in a mouse model of multistage carcinogenesis. Proc Natl Acad Sci USA. 2006; 103:12493–12498. [PubMed: 16891410]
23. Bekes EM, et al. Tumor-recruited neutrophils and neutrophil TIMP-free MMP-9 regulate coordinately the levels of tumor angiogenesis and efficiency of malignant cell intravasation. Am J Pathol. 2011; 179:1455–1470. [PubMed: 21741942]
24. Piccard H, Muschel RJ, Opdenakker G. On the dual roles and polarized phenotypes of neutrophils in tumor development and progression. Crit Rev Oncol Hematol. 2012; 82:296–309. [PubMed: 21798756]
25. Christoffersson G, et al. VEGF-A recruits a proangiogenic MMP-9-delivering neutrophil subset that induces angiogenesis in transplanted hypoxic tissue. Blood. 2012; 120:4653–4662. [PubMed: 22966168]

26. Massena S, et al. Identification and characterization of VEGF-A-responsive neutrophils expressing CD49d, VEGFR1, and CXCR4 in mice and humans. Blood. 2015; 126:2016–2026. [PubMed: 26286848]
27. Melero-Martin JM, et al. In vivo vasculogenic potential of human blood-derived endothelial progenitor cells. Blood. 2007; 109:4761–4768. [PubMed: 17327403]
28. Lin RZ, Chen YC, Moreno-Luna R, Khademhosseini A, Melero-Martin JM. Transdermal regulation of vascular network bioengineering using a photopolymerizable methacrylated gelatin hydrogel. Biomaterials. 2013; 34:6785–6796. [PubMed: 23773819]
29. Melero-Martin JM, et al. Host myeloid cells are necessary for creating bioengineered human vascular networks in vivo. Tissue Eng Part A. 2010; 16:2457–2466. [PubMed: 20218762]
30. Lin RZ, et al. Human endothelial colony-forming cells serve as trophic mediators for mesenchymal stem cell engraftment via paracrine signaling. Proc Natl Acad Sci USA. 2014; 111:10137–10142. [PubMed: 24982174]
31. Fridlender ZG, et al. Polarization of tumor-associated neutrophil phenotype by TGF-beta: “N1” versus ‘N2’ TAN. Cancer Cell. 2009; 16:183–194. [PubMed: 19732719]
32. Suchting S, et al. The Notch ligand Delta-like 4 negatively regulates endothelial tip cell formation and vessel branching. Proc Natl Acad Sci USA. 2007; 104:3225–3230. [PubMed: 17296941]
33. Roca C, Adams RH. Regulation of vascular morphogenesis by Notch signaling. Genes & Development. 2007; 21:2511–2524. [PubMed: 17938237]
34. White JR, et al. Identification of a potent, selective non-peptide CXCR2 antagonist that inhibits interleukin-8-induced neutrophil migration. J Biol Chem. 1998; 273:10095–10098. [PubMed: 9553055]
35. Mantovani A. The yin-yang of tumor-associated neutrophils. Cancer Cell. 2009; 16:173–174. [PubMed: 19732714]
36. Fridlender ZG, Albelda SM. Tumor-associated neutrophils: friend or foe? Carcinogenesis. 2012; 33:949–955. [PubMed: 22425643]
37. Sagiv JY, et al. Phenotypic diversity and plasticity in circulating neutrophil subpopulations in cancer. Cell Rep. 2015; 10:562–573. [PubMed: 25620698]
38. Fridlender ZG, et al. Transcriptomic analysis comparing tumor-associated neutrophils with granulocytic myeloid-derived suppressor cells and normal neutrophils. PLoS ONE. 2012; 7:e31524. [PubMed: 22348096]
39. Cuartero MI, et al. N2 neutrophils, novel players in brain inflammation after stroke: modulation by the PPARγ agonist rosiglitazone. Stroke. 2013; 44:3498–3508. [PubMed: 24135932]
40. Ma Y, et al. Temporal neutrophil polarization following myocardial infarction. Cardiovasc Res. 2016; 110:51–61. [PubMed: 26825554]
41. Fantin A, et al. Tissue macrophages act as cellular chaperones for vascular anastomosis downstream of VEGF-mediated endothelial tip cell induction. Blood. 2010; 116:829–840. [PubMed: 20404134]
42. Murdoch C, Giannoudis A, Lewis CE. Mechanisms regulating the recruitment of macrophages into hypoxic areas of tumors and other ischemic tissues. Blood. 2004; 104:2224–2234. [PubMed: 15231578]
43. Murdoch C, Muthana M, Coffelt SB, Lewis CE. The role of myeloid cells in the promotion of tumour angiogenesis. Nat Rev Cancer. 2008; 8:618–631. [PubMed: 18633355]
44. Benelli R, et al. Neutrophils as a key cellular target for angiostatin: implications for regulation of angiogenesis and inflammation. FASEB J. 2002; 16:267–269. [PubMed: 11772950]
45. Baranski JD, et al. Geometric control of vascular networks to enhance engineered tissue integration and function. Proc Natl Acad Sci USA. 2013; 110:7586–7591. [PubMed: 23610423]
46. Riemenschneider SB, et al. Inosculation and perfusion of pre-vascularized tissue patches containing aligned human microvessels after myocardial infarction. Biomaterials. 2016; 97:51–61. [PubMed: 27162074]
47. Ausprunk DH, Knighton DR, Folkman MJ. Vascularization of normal and neoplastic tissues grafted to the chick chorioallantois. Role of host and preexisting graft blood vessels. Am J Pathol. 1975; 79:597–618. [PubMed: 1094838]

48. Nolan DJ, et al. Molecular signatures of tissue-specific microvascular endothelial cell heterogeneity in organ maintenance and regeneration. Dev Cell. 2013; 26:204–219. [PubMed: 23871589]
49. Lee JH, et al. Lung stem cell differentiation in mice directed by endothelial cells via a BMP4-NFATc1-thrombospondin-1 axis. Cell. 2014; 156:440–455. [PubMed: 24485453]
50. Hu J, et al. Endothelial cell-derived angiopoietin-2 controls liver regeneration as a spatiotemporal rheostat. Science. 2014; 343:416–419. [PubMed: 24458641]
51. Kusumbe AP, Ramasamy SK, Adams RH. Coupling of angiogenesis and osteogenesis by a specific vessel subtype in bone. Nature. 2014; 507:323–328. [PubMed: 24646994]
52. Shen Q, et al. Endothelial cells stimulate self-renewal and expand neurogenesis of neural stem cells. Science. 2004; 304:1338–1340. [PubMed: 15060285]
53. Zhou P, et al. Interrogating translational efficiency and lineage-specific transcriptomes using ribosome affinity purification. Proc Natl Acad Sci USA. 2013; 110:15395–15400. [PubMed: 24003143]
54. Wang Y, et al. Ephrin-B2 controls VEGF-induced angiogenesis and lymphangiogenesis. Nature. 2010; 465:483–486. [PubMed: 20445537]
55. Lin RZ, et al. Induction of erythropoiesis using human vascular networks genetically engineered for controlled erythropoietin release. Blood. 2011; 118:5420–5428. [PubMed: 21937702]

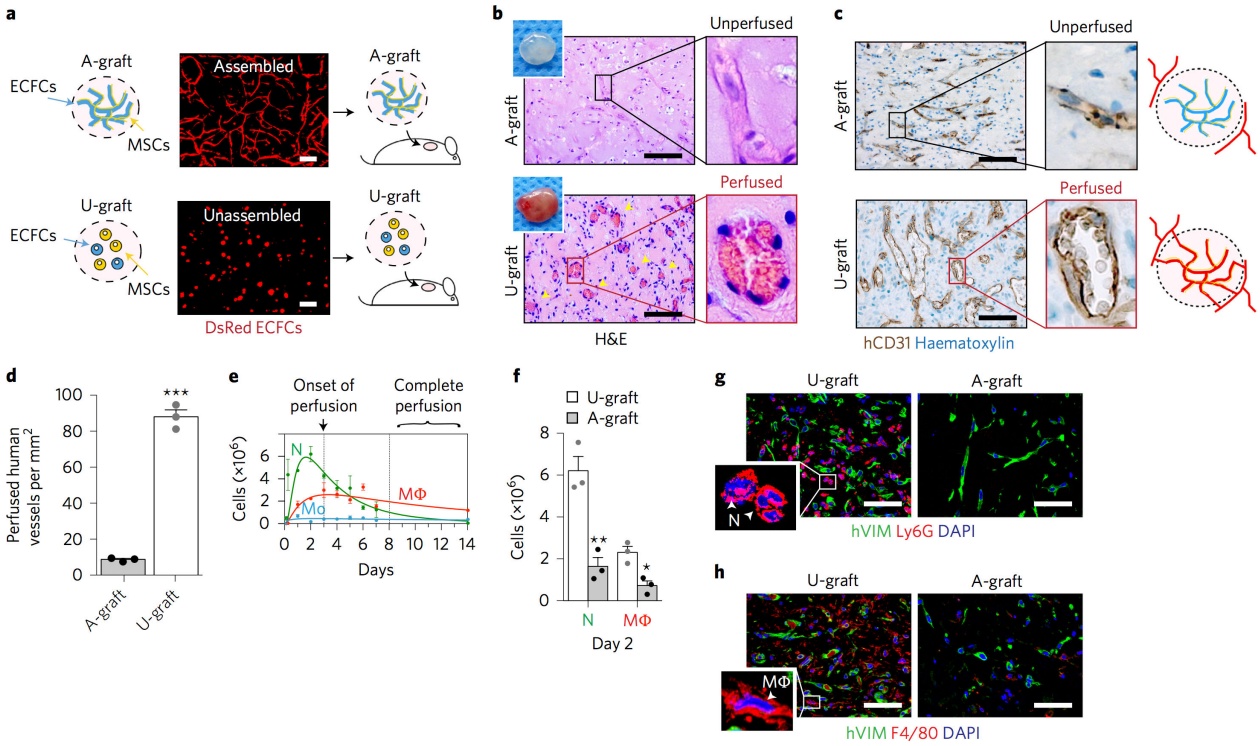

Figure 1. Engraftment of bioengineered microvascular networks

(**a**) Schematic of microvascular graft models. Grafts were prepared *in vitro* by combining human ECFCs with MSCs in hydrogels and then surgically implanted into nude mice. Assembled vascular grafts (A-grafts) were created over 7 days *in vitro*, whereas unassembled grafts (U-grafts) contained a suspension of cells. (**b**) H&E staining of A-Grafts and U-Grafts explanted after 7 days *in vivo*. Insets are macroscopic views of the explants. Perfused vessels were identified as luminal structures containing red blood cells (RBCs) (yellow arrowheads). (**c**) Immunohistochemical staining of h-CD31+ cells at day 7. Human h-CD31+ vascular structures were identified as either perfused (lumens containing RBC) or non-perfused (cord structures). (**d**) Density of perfused human blood vessels at day 7. Bars represent mean ± s.d.; n = 3 mice per group. *** $P < 0.001$ between A-Grafts and U-Grafts. (**e**) Time-course cytometric quantification of myeloid cell subpopulations in U-Grafts. (**f**) Cytometric quantification of neutrophils (N) and macrophages (MΦ) in U-Grafts and A-Grafts at day 2 post-implantation. Bars represent mean ± s.d.; n = 3 grafts per group. ** $P < 0.01$, * $P < 0.05$ between A-Grafts and U-Grafts. Immunofluorescent staining of (**g**) Ly6G+ neutrophils (red) and (**h**) F4/80+ macrophages (red) in U-Grafts and A-Grafts at day 2 post-implantation. Human cells visualized as h-vimentin+ cells (green). Nuclei stained by DAPI. Scale bars: 100 μm (b, c) and 50 μm (a, g, h).

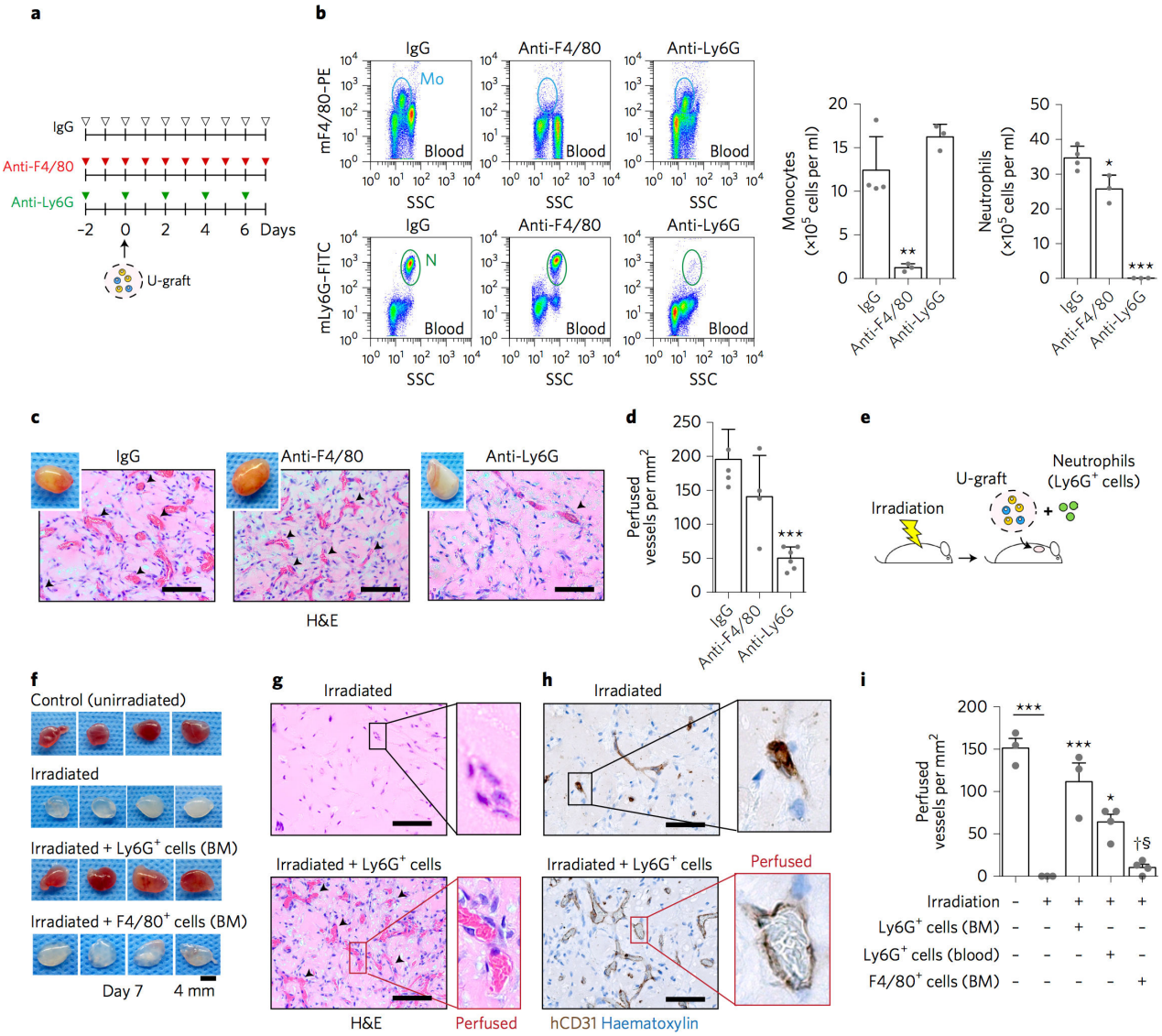

Figure 2. Host neutrophils are indispensable for graft vascularization

(**a**) Schematic with myeloid depletion strategies. Circulating monocytes depleted with α-F4/80 antibodies (α-F4/80). Neutrophils depleted with α-Ly6G antibodies (α-Ly6G). U-Graft implanted at day 0. Control (IgG antibodies) and treatments initiated at day −2 and maintained until day 7. (**b**) Flow cytometry analysis of blood samples 2 days after depletion treatments. Gates for circulating monocytes (Mo) and neutrophils (N) depicted. Bars represent mean ± s.d.; n = 3–4. *** $P < 0.001$, ** $P < 0.01$, * $P < 0.05$ compared to IgG group. (**c**) H&E staining of U-Grafts explanted at day 7. Insets are macroscopic views of the explants. Perfused vessels were identified as luminal structures containing RBCs (yellow arrowheads). (**d**) Density of perfused blood vessels at day 7. Bars represent mean ± s.d.; n = 4–6 mice per group. *** $P < 0.001$ compared to IgG group. (**e**) Schematic with neutrophil adoptive transfer strategy. U-Graft implanted into irradiated mice and neutrophils simultaneously transferred from non-irradiated donors. (**f**) Macroscopic views of U-Grafts explanted at day 7 from: (i) non-irradiated mice, (ii) irradiated mice, (iii) irradiated mice +

transfer of BM-Ly6G+ cells, and (iv) irradiate mice + transfer of BM-F4/80+ cells. (**g**) H&E and (**h**) immunohistochemical (h-CD31+ cells) staining of U-Grafts explanted at day 7 from irradiated mice with and without BM-Ly6G+ cell transfer. Perfused vessels marked by yellow arrowheads. (**i**) Microvessel density at day 7. Bars represent mean ± s.d.; n = 3–4 mice per group. *** $P < 0.001$, * $P < 0.05$ compared to irradiated group (no transfer). † $P < 0.001$ compared to irradiated + BM-Ly6G+ cell transfer. § $P < 0.05$ compared to irradiated + Blood-Ly6G+ cell transfer. Scale bars: 100 μm (c, g, h).

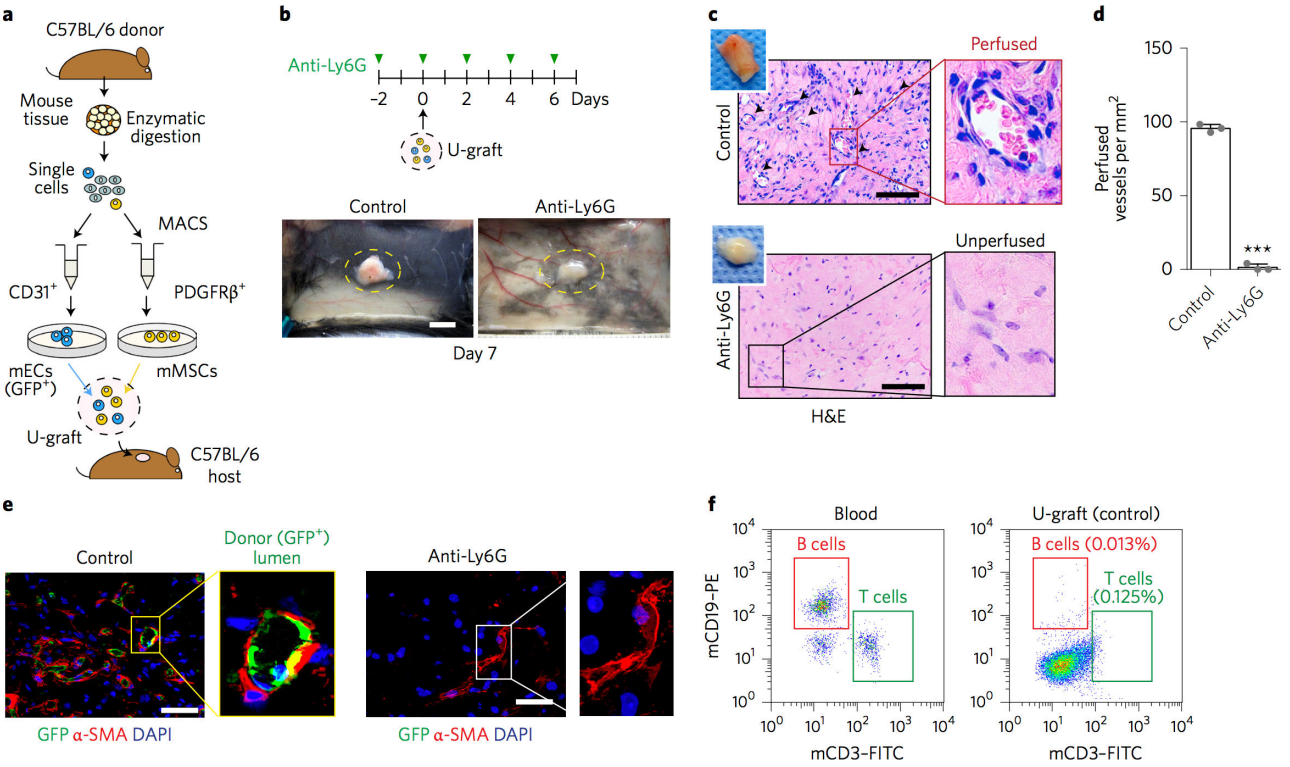

Figure 3. Host neutrophils are indispensable for graft vascularization in a syngeneic murine C57BL/6 model

(**a**) Schematic of syngeneic grafting model on C57BL/6 mice. Subcutaneous tissues from C57BL/6 mice were enzymatically digested into single cell suspension. Magnetic-activated cell sorting (MACS) was performed to purify mouse ECs (mECs; CD31+) and mouse MSCs (mMSCs; PDGFRβ+). mECs were lentivirally transduced to express GFP. GFP-mECs and mMSCs were then implanted as U-Grafts into host C57BL/6 mice. (**b**) Neutrophils were depleted with α-Ly6G antibodies in C57BL/6 mice. U-Graft containing GFP-mECs and mMSCs were implanted at day 0. Control (IgG antibody) and α-Ly6G treatments were initiated at day −2 and maintained until day 7. Lower panels show macroscopic views of the subcutaneous grafts at day 7. (**c**) H&E staining of U-Grafts explanted at day 7. Insets are macroscopic views of the explants. Perfused vessels were identified as luminal structures containing RBCs (yellow arrowheads). (**d**) Density of perfused blood vessels at day 7. Bars represent mean ± s.d.; n = 3 mice per group. *** $P < 0.001$ compared to control. (**e**) Vessels lined by donor mECs were identified by GFP and perivascular coverage by α-SMA+ staining. Nuclei stained by DAPI. (**f**) Flow cytometry analysis of murine U-Grafts implanted in C57BL/6 host. Cytometric analyses included blood samples and cells retrieved from explanted U-Grafts at day 2. B cells were identified as mCD19-positive cells and T cells as mCD3-positive. Scale bars: 4 mm (b) and 100 μm (c, e).

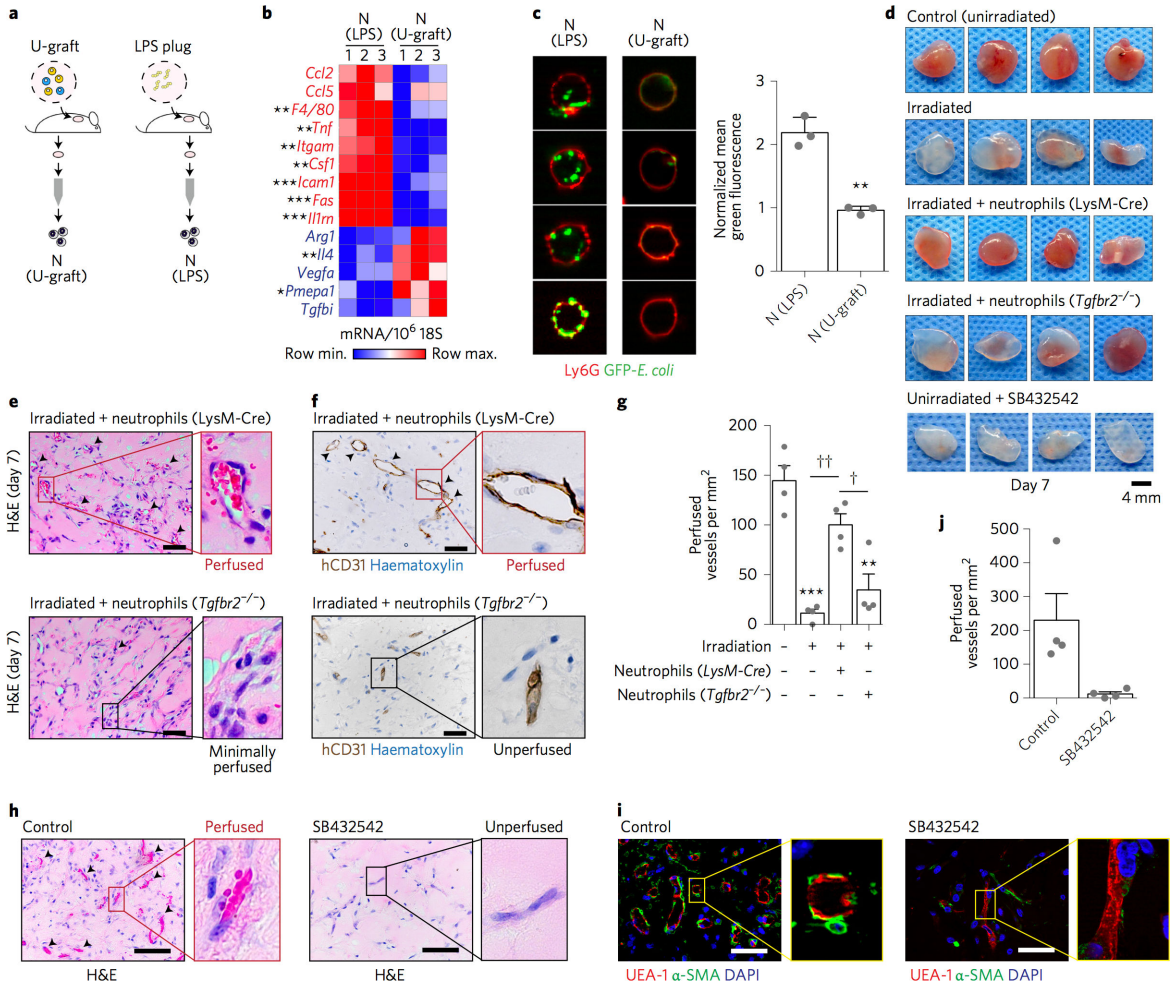

Figure 4. Alternatively polarized neutrophils mediate U-Graft vascularization

(**a**) Schematic with neutrophils (N) isolated from either explanted U-Grafts or from lipopolysaccharide (LPS)-containing plugs. (**b**) Heat map of gene expression levels (by qPCR) in neutrophils from U-Grafts and LPS plugs. Primers were mouse specific (Supplementary Table 2). mRNA data are row-relative and normalized to ribosomal 18S rRNA. n = 3 mice per group. *** $P < 0.001$, ** $P < 0.01$, * $P < 0.05$ between U-Graft and LPS groups. (**c**) Representative Ly6G+ (red) neutrophils from U-Grafts and LPS plugs after exposure to *gfp-E.coli* (green). Phagocytosis of *gfp-E.coli* was visualized under a fluorescent microscope and quantified by flow cytometry. Bars represent normalized mean green fluorescence ± s.d. measured in gated Ly6G+ neutrophils; n = 3 mice per group. ** $P < 0.01$ between U-Graft and LPS groups. (**d**) Macroscopic views of U-Grafts explanted at day 7 from: (i) non-irradiated mice, (ii) irradiated mice, (iii) irradiated mice + transfer of BM-*LysM-Cre*-neutrophils, (iv) irradiate mice + transfer of BM-*tgfbr2*$^{-/-}$ neutrophils, and (v) non-irradiated mice + TGF-β receptor inhibitor (SB432542). (**e**) H&E and (**f**) immunohistochemical (h-CD31+ cells) staining of U-Grafts explanted at day 7 from irradiated mice with transfer of either BM-*LysM-Cre* or BM-*tgfbr2*$^{-/-}$ neutrophils. Perfused vessels marked by yellow arrowheads. (**g**) Microvessel density at day 7. Bars represent mean ± s.d.; n = 4 mice per group. *** $P < 0.001$, ** $P < 0.01$ compared to non-irradiated control

group. † $P < 0.05$ and †† $P < 0.01$ between indicated groups. (**h–j**) U-Grafts were implanted in mice treated with SB432542. Mice receiving saline injections served as controls. (**h**) H&E staining of explanted U-Grafts at day 7. (**i**) Immunofluorescent staining revealed the presence of human vessels (UEA-1+ lumen) and perivascular coverage (α-SMA+ cells) in the control group; and non-perfused human endothelial cord structures in SB432542-treated grafts. (**j**) Microvessel density quantified at day 7. Bars represent mean ± s.d.; n = 4 mice per group. * $P < 0.05$. Scale bars: 100 μm (e, f, h, i).

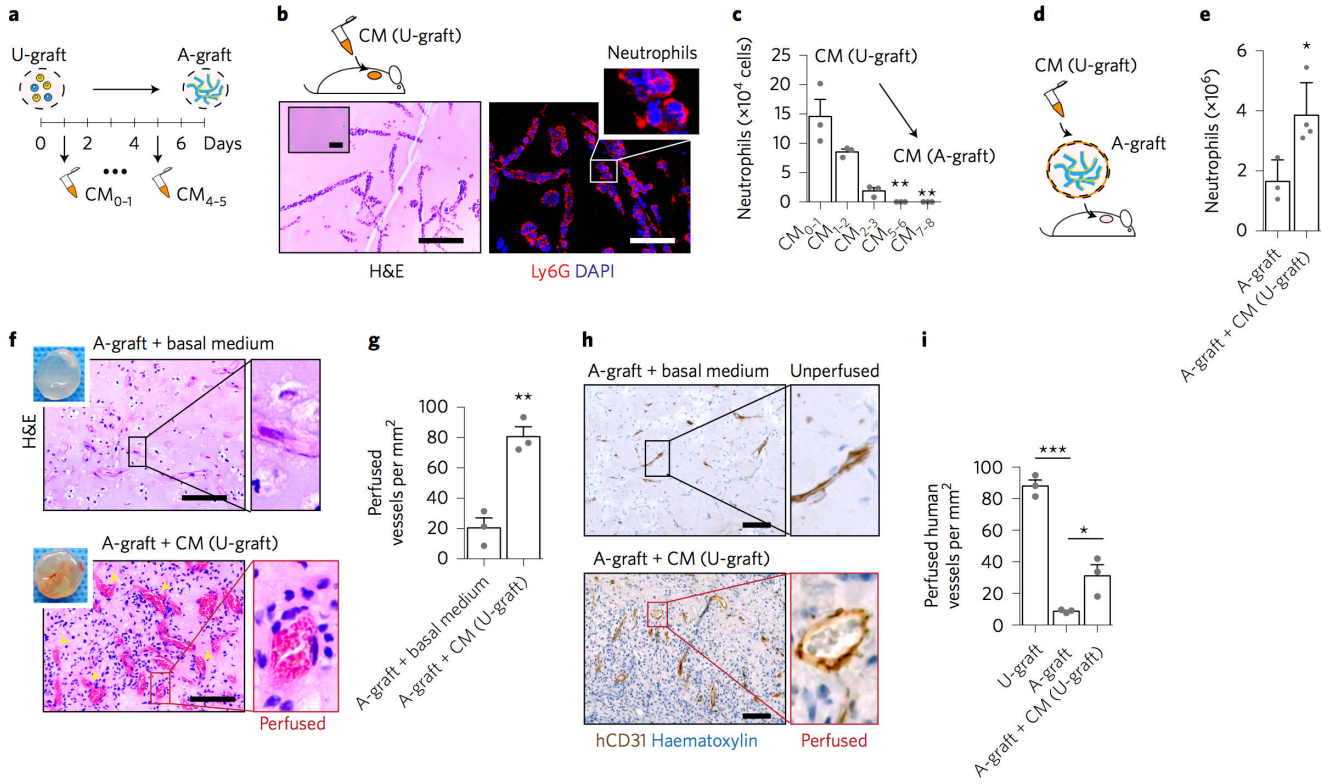

Figure 5. Neutrophil activity regulated by secreted factors from the graft vasculature

(**a**) Schematic: daily samples of conditioned media (CM) collected from U-Grafts until they became A-Grafts. (**b**) H&E (left) and immunofluorescent (Ly6G, DAPI) staining revealing infiltration of neutrophils at day 2 into implanted Matrigel plugs containing CM from U-Grafts. Left H&E inset corresponds to plug containing control basal medium (basal-M). (**c**) Flow cytometric quantification of neutrophil infiltration at day 2 into plugs containing CM collected at indicated times. Bars represent mean ± s.d.; n = 3 plugs per group. ** $P < 0.01$, * $P < 0.05$ compared to $CM_{0–1}$. (**d**) Schematic of A-Grafts impregnated in CM from U-Grafts and implanted into nude mice. (**e**) Flow cytometric quantification of neutrophil infiltration at day 2 into A-Grafts that were impregnated with and without CM(U-Graft). (**f**) H&E staining at day 7 of explanted A-Grafts that were impregnated with either CM(U-Graft) or basal-M. Insets are macroscopic views of the explants. Perfused vessels marked by yellow arrowheads. (**g**) Microvessel density at day 7. Bars represent mean ± s.d.; n = 3 mice per group. ** $P < 0.01$. (**h**) Immunohistochemical staining (h-CD31+ cells) at day 7 in explanted A-Grafts that were impregnated with either CM(U-Graft) or basal-M. Perfused human h-CD31+ vascular structures were identified as lumens containing RBC. (**i**) Density of perfused human microvessels at day 7. Bars represent mean ± s.d.; n = 3 mice per group. *** $P < 0.001$, * $P < 0.05$ between indicated groups. Scale bars: 100 μm (b left, f, h), 50 μm (b right).

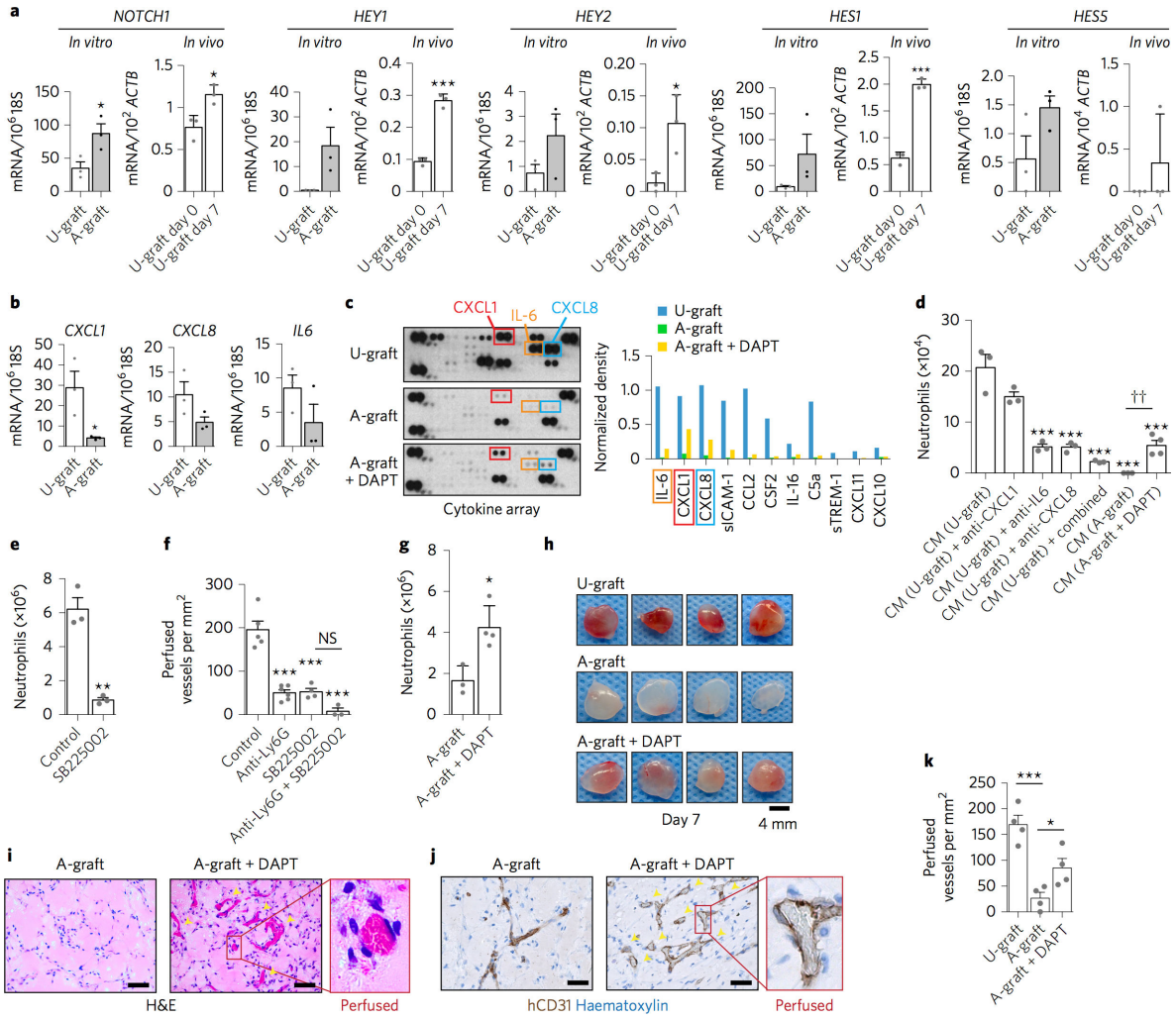

Figure 6. Notch inhibition promotes A-Graft revascularization

(**a**) mRNA gene expression (qPCR) of NOTCH1 and downstream mediators of Notch signalling pathway (HEY1, HEY2, HES1, HES5). *In vitro*: data from ECFCs retrieved from U-Grafts and A-Grafts and normalized to ribosomal 18S rRNA. *In vivo*: data from total mRNA isolated from U-Grafts 30 min (day 0) and 7 days after implantation. Data normalized to human β-actin (ACTB). Bars represent mean ± s.d.; n = 3 grafts per group. *** $P < 0.001$, * $P < 0.05$. (**b**) Expression of *CXCL1*, *CXCL8*, and *IL6* in ECFCs retrieved from U-Grafts and A-Grafts and normalized to ribosomal 18S rRNA. (**c**) Human cytokine protein array analysis of conditioned media (CM) from U-Grafts, A-Grafts, and A-Grafts + DAPT (γ-secretase inhibitor; 24 h exposure). Selected cytokines marked with color-lined boxes. Quantification of cytokine levels were carried out by densitometry. (**d**) Blocking neutrophil recruitment by neutralizing antibodies in subcutaneous plug assays. Neutralizing antibodies against IL6, CXCL8, and CXCL1 were added to CM(U-Grafts) prior to implantation. The number of neutrophils recruited into the plugs were measured by flow cytometry at day 2. Bars represent mean ± s.d.; n = 3–4 mice per group. *** $P < 0.001$ compared to CM(U-Grafts). (**e**, **f**) Effect of CXCR2 antagonist (SB225002) on neutrophil recruitment and U-Graft vascularization. U-Grafts implanted in untreated mice served as

control. (**e**) Neutrophil recruitment into U-Graft at day 2 measured by flow cytometry. (**f**) Density of perfused microvessels at day 7. Bars represent mean ± s.d.; n = 3–6 mice per group. *** $P < 0.001$, ** $P < 0.01$ compared to Control. (**g**) Neutrophil recruitment at day 2 in A-Grafts and A-Grafts + DAPT. Bars represent mean ± s.d.; n = 3–4 mice per group. * $P < 0.05$. (**h**) Macroscopic views of U-Grafts, A-Grafts, and A-Grafts + DAPT, explanted at day 7. (**i**) H&E and (**j**) immunohistochemical (h-CD31+ cells) staining of A-Grafts and A-Grafts + DAPT explanted at day 7. Perfused vessels identified as luminal structures containing RBCs (yellow arrowheads). (**k**) Microvessel density at day 7. Bars represent mean ± s.d.; n = 4 mice per group. *** $P < 0.001$, * $P < 0.05$ between indicated groups. Scale bars: 50 μm.